VIII. BME STUDIES OF STOCHASTIC DIFFERENTIAL EQUATIONS REPRESENTING PHYSICAL LAW

A wide variety of natural processes are described using physical laws. A physical law may be expressed by means of an algebraic equation or a differential equation governing the physical process. Classical methods of Geostatistics have been designed to use mainly statistical knowledge about natural variables and they lack the ability to incorporate physical laws in the mapping analysis. On the other hand, BME can accomplish such a task, rigorously and accurately. Within the BME epistemic framework, these laws constitute general knowledge. As a consequence, the analysis at the prior BME stage is conditioned by the laws that govern the physical processes. Then the posterior BME stage is performed as usual, allowing to integrate case-specific data (such as measurements and uncertain observations).

In this chapter we discuss a general framework that permits to incorporate physical laws expressed in various forms, i.e., by means of algebraic functions or differential equations. We then illustrate the principles presented by means of a theoritical and numerical example. Finally the power of this approach is demonstrated in a ground water case study. In this case study, BME is used to incorporate the Darcy law of subsurface hydrology in the spatial mapping of a hydraulic head field. The hydraulic map thus obtained is physically meaningful as well as numerically more accurate than that obtained using classical methods (e.g., kriging). Moreover, by taking advantage of the Darcy law, the BME hydraulic head mapping can involve other related soil properties, like hydraulic conductivity. The approach leads to very accurate hydraulic head solutions, and may be

also applied to study the inverse problem, in which one seeks to estimate hydraulic conductivity from hydraulic head measurements.

8.1. Introduction

Physical laws expressed by mathematical equations govern the evolution of natural processes in space/time. Thus, they provide an important source of general knowledge G that can be used to complement the specific knowledge of the natural process derived from the available data and other sources. For example an advection model provides valuable information for managing uncertainty in an air quality GIS (Hassan and Huang, 1996). In the BME framework, physical laws are incorporated in the general knowledge by means of an appropriate set of moment equations (Christakos, 1998b, 1999; Christakos, Hristopulos and Serre, 1999). These moment equations contain the knowledge of the physical law, and they are naturally incorporated in the prior pdf of BME analysis. Incorporation of general knowledge in the mapping process can lead to considerable gains in accuracy and flexibility. For example the incorporation of the Darcy law in the mapping of water table elevations leads to predictions that are physically meaningful and more accurate than that provided by classical data analysis that does not account for the physical law (Serre and Christakos, 1999a).

In this work two prime classes of laws are considered: They are laws expressed as algebraic equations, and laws expressed as differential equations. Algebraic equations usually express an algebraic dependence between the primary Random Field (RF) $X(\boldsymbol{p})$ and a secondary (physically related) RF, $Y(\boldsymbol{p})$. Differential equations are a generalization of algebraic equation which also contain some differential operator expressing the space/time evolution of the primary RF $X(\boldsymbol{p})$. In this chapter we outline an approach

allowing to incorporate physical laws of algebraic and differential types, and we then demonstrate the approach by means of examples and case study.

8.2. Incorporating Physical Laws in BME mapping

We only give here a brief outline of the general framework for incorporating a physical law in the general knowledge, for a more detailed explanation see Christakos (1998a, 1999), and Christakos, Hristopulos and Serre (1999). We consider a physical variable represented by the random field (RF) $X(\boldsymbol{p})$ at the point $\boldsymbol{p} = (\boldsymbol{s}, t)$ in space/time, and we let $Y(\boldsymbol{p})$ be a secondary RF. The vector $\boldsymbol{x}_{\text{map}}$ is a representation of the RF at a set $\boldsymbol{p}_{\text{map}}$ of mapping points that includes both the *data* and the *estimation* points. As presented in Chapter VI, Eq. (6.5), the general knowledge available is processed in the BME framework by means of *moment equations* $\overline{g_\alpha(\boldsymbol{p}_{\text{map}})} = \int d\boldsymbol{\chi}_{\text{map}}\, d\boldsymbol{\psi}_{\text{data}}\, f_G(\boldsymbol{\chi}_{\text{map}}, \boldsymbol{\psi}_{\text{data}}; \boldsymbol{p}_{\text{map}}) g_\alpha(\boldsymbol{\chi}_{\text{map}}, \boldsymbol{\psi}_{\text{data}}), \quad \alpha = 0,1,\ldots,N_c,$ where $\boldsymbol{\chi}_{\text{map}}$ and , $\boldsymbol{\psi}_{\text{data}}$ denote specific realizations of $\boldsymbol{x}_{\text{map}}$ and $\boldsymbol{y}_{\text{data}}$, $f_G(\boldsymbol{\chi}_{\text{map}}, \boldsymbol{\psi}_{\text{data}}; \boldsymbol{p}_{\text{map}})$ is their joint *prior* pdf, and the g_α's are appropriate functions of $\boldsymbol{x}_{\text{map}}$ and $\boldsymbol{y}_{\text{data}}$ such that their expected values $\overline{g_\alpha}$ are known. These expected values $\overline{g_\alpha}$ may be determined directly from field data and experimental surveys (as considered in previous chapters), or they may be inferred from the physical law. A physical law can be expressed as either algebraic relations or differential equations.

Algebraic Relations:

In this case the physical law may be expressed in the form $\Phi(X(\boldsymbol{p}), Y(\boldsymbol{p})) = 0,$ where $\Phi(.)$ is an algebraic equation. This type of equation provides valuable information about the RF $X(\boldsymbol{p})$, however in order to incorporate it in the general knowledge, we must transform it into a set of moment equations. This is easily done by taking the stochastic expectation of the algeabric equation written at the mapping points $\boldsymbol{p}_i,\ i = 1,\ldots,n,$ where

$\boldsymbol{p}_i \in \boldsymbol{p}_{\text{map}}$. Hence the moment equations are obtained by writing $g_i(\boldsymbol{\chi}_{\text{map}}, \boldsymbol{\psi}_{\text{data}}) = \Phi_i(x_i; y_i)$ and $\overline{g_i} = 0$, $i = 1,...,n$, where x_i and y_i represent the RFs $X(\boldsymbol{p})$ and $Y(\boldsymbol{p})$, respectively, at point $\boldsymbol{p}_i$. These moment equations are readily incorporated in the general knowledge, as shown in previous chapters. Note that additional moment equations may as well be generated from the algebraic equation by considering the product of the algebraic equation written at all possible pairs of points (Christakos, Hristopulos and Serre, 1999).

Differential Equations

This category of physical laws includes ordinary (ODE) and partial differential equations (PDEs) that can be expressed in the general form $\Phi(X(\boldsymbol{p}), Y(\boldsymbol{p})) = D_{\boldsymbol{p}}[X(\boldsymbol{p})]$, where $D_{\boldsymbol{p}}$ is a space/time differential operator and Φ an algebraic function. If the PDE is solved explicitly by $X = H(\boldsymbol{Y})$ the problem is reduced to the previous case. If an algebraic solution is intractable, the differential equation can be still used in BME analysis by writing $g_i(\boldsymbol{\chi}_{\text{map}}, \boldsymbol{\psi}_{\text{data}}) = \Phi(X(\boldsymbol{p}_i), Y(\boldsymbol{p}_i))$ and $\overline{g_i} = \overline{D_{\boldsymbol{p}_i}[X(\boldsymbol{p}_i)]}$. Note that this approach is attractive because it does not require an explicit solution for the differential equation, however it will result in an implementation with a higher numerical complexity than in the previous case.

8.3. A Numerical Example For The Incorporation Of A Physical Law In The General Knowledge

In this numerical example (Serre and Christakos, 1999), we consider a physical law describing the evolution of natural process $X(t)$ in time. Using the BME framework, we show how to numerically implement the incorporation of the physical law in the general knowledge G, and obtain the G-based prior pdf $f_G(\chi; t)$ for the RF $X(t)$ at time t.

8.3.1. The physical law and the BME framework

Let's consider the following physical law describing the evolution of the natural process $X(t)$ in time,

$$rX(t) = \frac{dX(t)}{dt}, \tag{8.22}$$

where $X(t)$ is a RF depending on time t, with random initial condition $X(t) = X_0$. In this numerical example we show how to numerically implement the incorporation of the physical law (8.22) in the general knowledge, and obtain the prior pdf $f_G(\chi;t)$ for the RF $X(t)$ at time t. In the BME framework for physical laws, we take the stochastic expectation of some linear combination of the physical law, in order to derive suitable moment equations. Taking the stochastic expectation of (8.22) and of (8.22) multiplied by $X(t)$ yields the equations $r\overline{X(t)} = \frac{d\overline{X(t)}}{dt}$ and $r\overline{X^2(t)} = \frac{1}{2}\frac{d\overline{X^2(t)}}{dt}$, respectively. These moments are incorporated in the general knowledge by using the following g_α-functions

$$\left.\begin{aligned} & g_0 = 1;\ \overline{g_0} = 1 \\ & g_1 = rX(t);\ \overline{g_1} = \frac{\overline{dX(t)}}{dt} \\ & g_2 = rX^2(t);\ \overline{g_2} = \frac{1}{2}\frac{\overline{dX^2(t)}}{dt} \end{aligned}\right\}, \tag{8.23}$$

where by convention $g_0 = 1$ and $\overline{g_0} = 1$ define the normalization constraint. Using the moment equations (8.23) we may write the prior pdf as

$$f_G(\chi;t) = \exp[\mu_0(t) + \mu_1(t) r\chi + \mu_2(t) r\chi^2], \tag{8.24}$$

where the Lagrange coefficients are obtained by using the constraints (8.23). Using the expression for $f_G(\chi;t)$ we may write these constraints as follow

$$\left.\begin{aligned} &\int d\chi\, f_G(\chi;t) = 1 \\ &\int d\chi\, r\chi\, f_G(\chi;t) = \int d\chi\, \chi \frac{df_G(\chi;t)}{dt} \\ &\int d\chi\, r\chi^2\, f_G(\chi;t) = \frac{1}{2}\int d\chi\, \chi^2 \frac{df_G(\chi;t)}{dt} \end{aligned}\right\}. \tag{8.25}$$

The first equation in (8.25) gives the normalization constraint as $\exp\mu_0(t) = 1/\int d\chi \exp[\mu_1(t) r\chi + \mu_2(t) r\chi^2]$. The time derivative of $f_G(\chi;t)$ is given by $\frac{df_G(\chi;t)}{dt} = (\frac{d\mu_0(t)}{dt} + \sum_{k=1}^{2} r\chi^k \frac{d\mu_k(t)}{dt}) f_G(\chi;t)$. It is usefull to note that $\frac{d}{dt}\int d\chi\, f_G(\chi;t) = \frac{d\mu_0(t)}{dt} + \sum_{k=1}^{2} r \frac{d\mu_k(t)}{dt} \int d\chi\, \chi^k\, f_G(\chi;t) = 0$, and after some manipulations we obtain that $\frac{df_G(\chi;t)}{dt} = \sum_{k=1}^{2} (r\chi^k - rM_k(t)) \frac{d\mu_k(t)}{dt} f_G(\chi;t)$, where

$$M_k(t) = \int d\chi\, \chi^k\, f_G(\chi;t) = \frac{\int d\chi\, \chi^k \exp[\mu_1(t) r\chi + \mu_2(t) r\chi^2]}{\int d\chi \exp[\mu_1(t) r\chi + \mu_2(t) r\chi^2]},\ k = 1,2\,. \tag{8.26}$$

Using this result we may rewrite the second and third equation of (8.25) as

$$M_i(t) = \frac{1}{i}\sum_{k=1}^{2} (M_{k+i}(t) - M_k(t) M_i(t)) \frac{d\mu_i(t)}{dt},\ k = 1,2\,. \tag{8.27}$$

It is convenient for numerical purposes to express Eq. (8.27) in matrix form as follow

$$\boldsymbol{D}[\boldsymbol{\mu}(t)] = \boldsymbol{H}[\boldsymbol{\mu}(t)] \frac{d}{dt}\boldsymbol{\mu}(t), \tag{8.28}$$

where $\boldsymbol{\mu}(t) = [\mu_1(t)\ \ \mu_2(t)]^{\mathrm{T}}$, $\boldsymbol{D}[\boldsymbol{\mu}(t)] = [M_1(t)\ \ M_2(t)]^{\mathrm{T}}$, and $\boldsymbol{H}[\boldsymbol{\mu}(t)] = \begin{bmatrix} M_2(t) - M_1(t)M_1(t) & M_3(t) - M_2(t)M_1(t) \\ (M_3(t) - M_2(t)M_1(t))/2 & (M_4(t) - M_2(t)M_2(t))/2 \end{bmatrix}$. The Lagrange coefficients are then easily calculated by solving numerically $\frac{d}{dt}\boldsymbol{\mu}(t) = \boldsymbol{H}^{-1}[\boldsymbol{\mu}(t)]\boldsymbol{D}[\boldsymbol{\mu}(t)]$, using the initial condition $\boldsymbol{\mu}(0) = [\mu_{1,0}\ \ \mu_{2,0}]^{\mathrm{T}}$. The forward difference approximation is well suited for this application and it is given by

$$\boldsymbol{\mu}(t_{i+1}) \cong \boldsymbol{\mu}(t_i) + (t_{i+1} - t_i)\boldsymbol{H}^{-1}[\boldsymbol{\mu}(t_i)]\boldsymbol{D}[\boldsymbol{\mu}(t_i)]. \tag{8.29}$$

8.3.2. Numerical results

The initial value X_0 for the RF $X(t)$ at time $t = 0$ is a random variable. We assume that at t=0, the distribution of X_0 is described by the following pdf

$$f_G(\chi;0) = \exp[\mu_0(0) + \mu_1(0)r\chi + \mu_2(0)r\chi^2], \tag{8.30}$$

with $\mu_0(0) = -90.3964$, $\mu_1(0)r = 19.539$ and $\mu_2(0)r = -1.0622$. This corresponds approximately to a mean of $m_0 = 9.1974$ and a variance of $\sigma_0^2 = 0.4707$. At time $t > 0$, we assume that the evolution of $X(t)$ is governed by the physical law $dX(t)/dt = rX(t)$, where the coefficient r is given by r=-0.01.

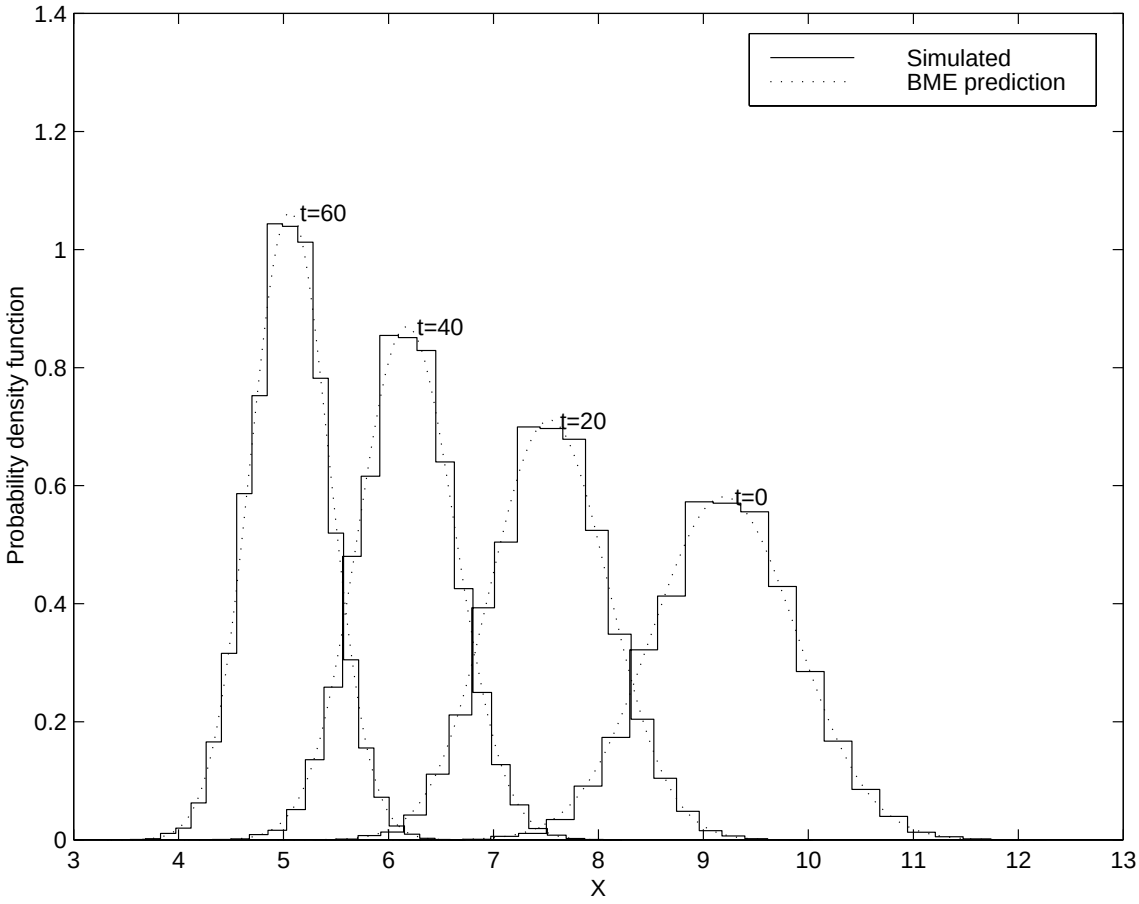

Figure 8.1: Probability density function of $X(t)$ at times $t = 0$, $t = 20$, $t = 40$, and $t = 60$. The pdf from simulated values are in plain line, and the BME pdf are in dotted lines.

Using the initial pdf, Eq. (8.30), we generate 10000 values of the initial value X_0. The histogram of the simulated values is shown in figure 8.1 in plain line, while the theoretical pdf (Eq. 8.30), is shown in dotted line at t=0. In the BME framework we calculate the Lagrange coefficients $\mathbf{\mu}(t) = [\mu_1(t)\ \ \mu_2(t)]^{\mathrm{T}}$ for the BME prior pdf $f_G(\chi;t)$ by solving Eq. (8.29) with a time step of $dt = 0.05$ time units. The calculated Lagrange coefficients are shown in Fig. 8.2. for time values up to $t = 60$.

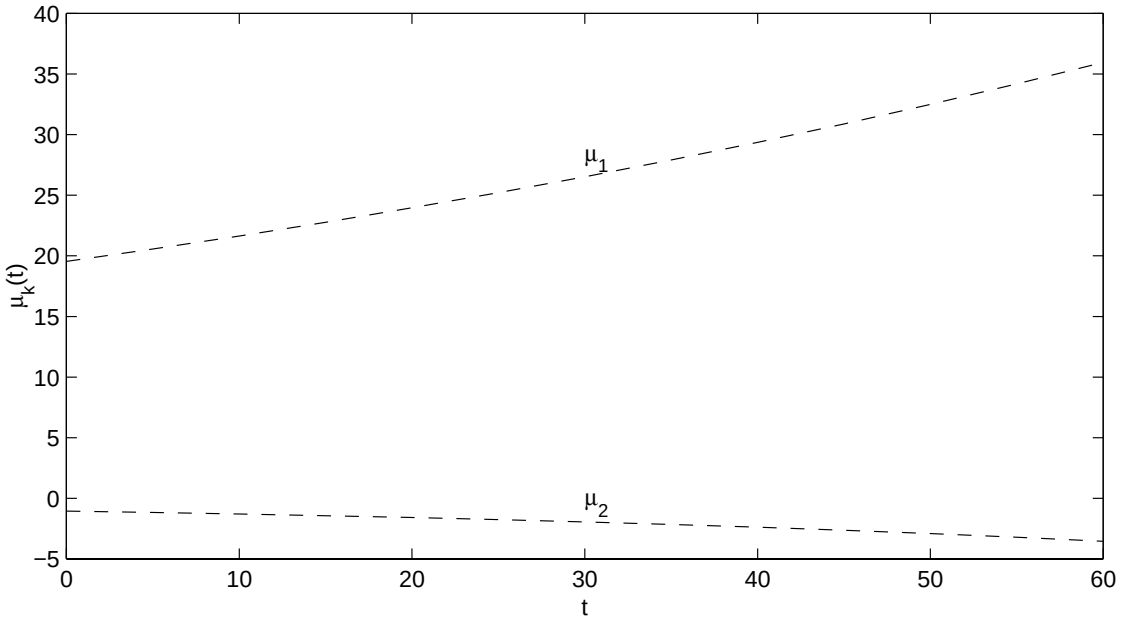

Figure 8.2: Calculated Lagrange coefficients $\boldsymbol{\mu}(t) = [\mu_1(t)\ \ \mu_2(t)]^{\mathrm{T}}$

For comparison purposes, we may calculate at a given time t the value $X_{t,1} = X_{0,1} \exp rt$ corresponding to each simulated initial value $X_{0,1}$, where $1 = 1,...,10000$ is the simulation number. In Fig. 8.1 we show the histogram (in plain line) of the $X_{t,1}$ values at times $t = 20$, $t = 40$, and $t = 60$. Also shown in the figure in dotted line are the theoretical pdfs $f_G(\chi;t) = \exp[\mu_0(t) + \mu_1(t) r\chi + \mu_2(t) r\chi^2]$ corresponding to the calculated Lagrange coefficients $\boldsymbol{\mu}(t) = [\mu_1(t)\ \ \mu_2(t)]^{\mathrm{T}}$ at times $t = 20$, $t = 40$, and $t = 60$. As one can see from the figure, the predicted BME pdfs are in good agreement with the simulated histograms.

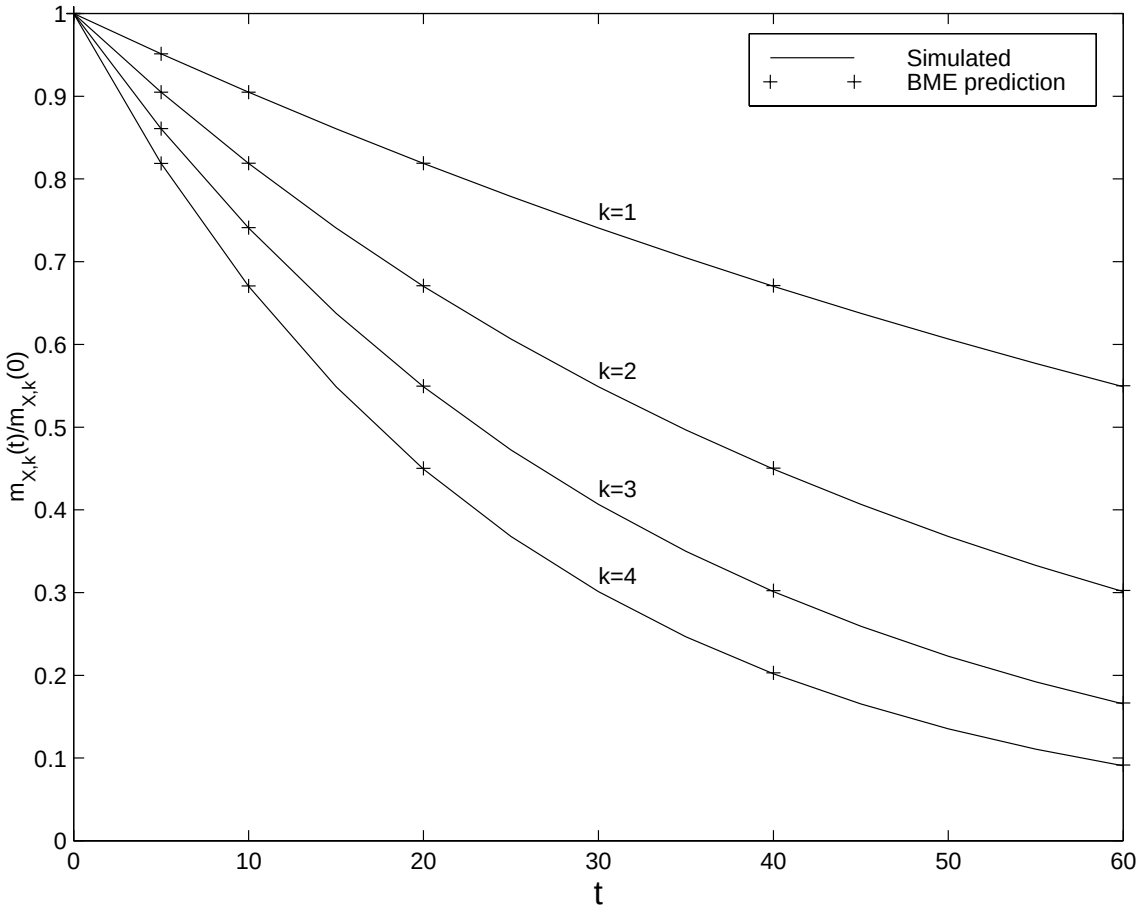

Figure 8.3: Normalized non-centered moments $m_{x,k}(t)/m_{x,k}(0)$ of order $k=1,...,4$ calculated using the simulated values (plain line), and the BME pdf (crosses).

Additionally we may calculate the statistical moments for $X(t)$ at a given time, using both the simulated values $X_{t,1}$, $1=1,...,10000$, and the BME pdf $f_G(\chi;t)$. In Fig. 8.3 we show the non-centered moments $m_{x,k}(t)=\overline{X^k(t)}$ of order $k=1,...,4$ calculated using the simulated values (plain line), and the BME pdf (crosses). In Fig. 8.4 we show the centered moments $c_{x,k}(t)=\overline{(X(t)-\overline{X}(t))^k}$ of order $k=2,...,4$ calculated using the simulated values (plain line), and the BME pdf (crosses). It is apparent from these figures that the BME pdf predicts correctly the moments of $X(t)$. Hence the BME framework allows to accurately incorporate a physical law in the general knowledge.

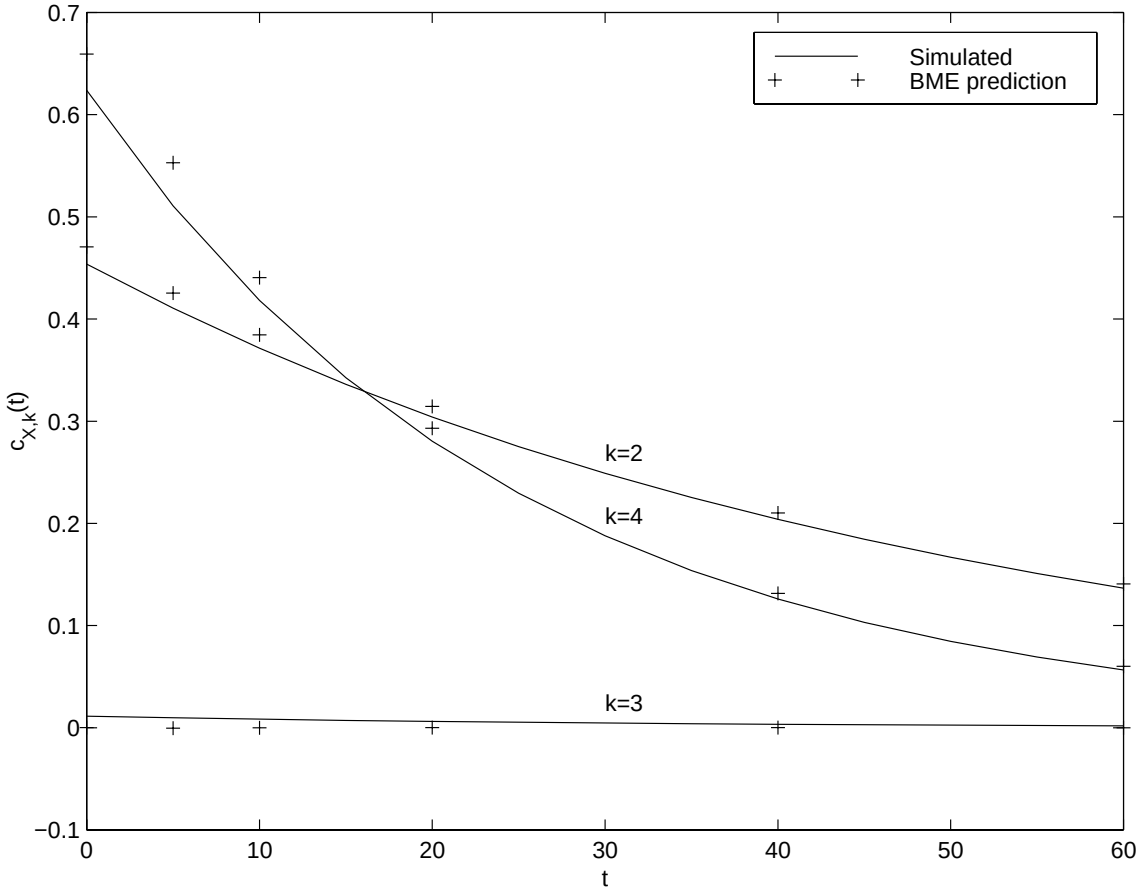

Figure 8.4: Centered moments $c_{x,k}(t) = \overline{(X(t) - \overline{X}(t))^k}$ of order $k = 2,...,4$ calculated using the simulated values (plain line), and the BME pdf (crosses).

In this example we have shown how the BME framework allows to incorporate a physical law in the general knowledge G, which leads to a G-based prior pdf $f_G(\boldsymbol{\chi}_{map})$. In BME mapping, the specificatory knowledge S (consisting of hard and soft data) is then used to update the prior pdf, leading to the posterior pdf useful for spatiotemporal mapping. In the next section we present a numerical case study for the mapping of water-table elevation, which shows the incorporation of the physical law at the prior stage as well as the processing of the hard and soft data at the posterior stage.

8.4. BME Mapping of Unidimentional Ground water Flow

Flow in porous media is described by the Darcy law, which relates hydraulic conductivity and hydraulic heads. Darcy law is an important part of the general knowledge available to hydrologists. In this numerical case study we demonstrate the power of the BME approach in the case of unidirectional ground water flow. In the BME approach, the Darcy law is integrated in the general knowledge describing the hydraulic head (water table elevation) of an aquifer. The general knowledge is used in the prior stage of the BME method which provides a prior pdf describing the joint distribution of hydraulic head and hydraulic conductivity. In the posterior stage of the BME approach, specificatory knowledge is used to update the prior pdf and leads to the posterior pdf useful for mapping applications.

8.4.1. A Formulation of the One-Dimensional Flow Problem

Consider the Darcy law for unidirectional flow

$$q(s) = -K(s)\frac{dH(s)}{ds}, \tag{8.31}$$

where the specific discharge $q(s)$ is considered deterministic while the hydraulic head $H(s)$ and the hydraulic conductivity $K(s)$ are random fields. It is convenient to rewrite the Darcy law as follow

$$\frac{dH(s)}{ds} = -q(s)\ R(s), \tag{8.32}$$

where $R(s) = 1/K(s)$ is the hydraulic resistivity random field. Eq. (8.32) is a Stochastic Ordinary Differential Equation (SODE) with the following boundary condition

$$\begin{cases} q(s) \\ H(0) = H_0 \end{cases}, \tag{8.33}$$

i.e. we assume that hydraulic head profile $H(s)$ has a known value H_0 at the origin s=0.

The hydraulic resistivity $R(s)$ is a property of the porous media that is governed by soil formation and geology. This soil property is characterized by its statistical moments, which are usually obtained from experimental data. In particular we assume that the hydraulic resistivity has a known mean $m_R(s)$ and non-centered covariance function $m_{R,2}(s,s')$, so that we may write

$$\begin{cases} \overline{R(s)} = m_R(s) \\ \overline{R(s)R(s')} = m_{RR}(s,s') \end{cases}, \tag{8.34}$$

and the variance of $R(s)$ is given by $\sigma_R^2(s) = m_{RR}(s,s) - m_R^2(s)$. If we assume that the hydraulic resistivity has a known fourth order non-centered moment $m_{R,4}(s)$ we may additionally write

$$\overline{R^4(s)} = m_{R,4}(s). \tag{8.35}$$

The statistical moments of the hydraulic resistivity are a function of the geomorphology of the soil and are usually obtained from experimental data. On the other hand the moments describing the hydraulic head are obtained from the Darcy law, Eq. (8.32). Using the Darcy law we may obtain expression for the mean $m_H(s) = \overline{H(s)}$ and non-centered covariance function $\overline{H(s)H(s')} = m_{HH}(s,s')$ of the hydraulic head, as well as the non-centered cross-covariance function $\overline{R(s)H(s')} = m_{RH}(s,s')$, as shown in the next section.

8.4.2. Using Darcy Law to Obtain Hydraulic Head Moments

Taking the expected value of Eq. (8.32) we obtain the equation

$$\frac{d}{ds}\overline{H}(s) = -q(s)\, m_R(s). \tag{8.36}$$

Solving for the mean hydraulic head $m_H(s) = \overline{H}(s)$ and using the boundary condition (8.33), we obtain that

$$m_H(s) = H_o - \int_0^s du\, q(u)\, m_R(u). \tag{8.37}$$

Multiplying Eq. (8.32) taken at s by $R(s')$ and then taking the expected value, we have

$$\frac{d}{ds} m_{HR}(s,s') = -q(s)\, m_{RR}(s,s'), \tag{8.38}$$

where $q(s)$ and $m_{RR}(s,s')$ are known functions. The solution of Eq. (8.38) is given, after considering the boundary condition of Eq. (8.33), by

$$m_{HR}(s,s') = H_0 m_R(s') - \int_0^s du\, q(u)\, m_{RR}(u,s') \tag{8.39}$$

Finally, multiplying Eq. (8.32) taken at s by $H(s')$ and then taking the expected value, we get

$$\frac{d}{ds} m_{HH}(s,s') = -q(s)\, m_{HR}(s',s), \tag{8.40}$$

the solution of which is given, after substituting Eq. (8.39) into Eq. (8.40) and considering the boundary condition of Eq. (8.33), by

$$m_{HH}(s,s') = \int_0^s du \int_0^{s'} du'\, q(u)\, q(u')\, m_{RR}(u,u') - H_0^2 + H_0(m_H(s) + m_H(s')) \qquad (8.41)$$

The statistical moments involving the hydraulic head, $m_H(s)$, $m_{HH}(s,s')$ and $m_{HR}(s,s')$, represent the knowledge provided by the Darcy law, Eq. (8.32). This knowledge is incorporated in the BME approach by defining an appropriate set of constraints g_α, and obtaining the prior pdf which maximizes expected information subject to these constraints, as shown next.

8.4.3. The BME Prior PDF

Let $\boldsymbol{H}_{\text{map}} = [H_1,...,H_{n_H}]^{\text{T}}$ be the vector of random variable representing the hydraulic head $H(s)$ at points $s_1,...,s_{n_H}$, and $\boldsymbol{R}_{\text{data}} = [R_{n_H+1},...,R_n]^{\text{T}}$ be the vector of random variables representing the hydraulic resistivity $R(s)$ at points $s_{n_H+1},...,s_n$. At the prior stage of the BME analysis we seek to obtain the prior pdf $f_G(H_{\text{map}}, R_{\text{data}}; s_1...s_n)$ given general knowledge G (which includes the Darcy law), where H_{map} and R_{data} represent a realization of the random vectors $\boldsymbol{H}_{\text{map}}$ and $\boldsymbol{R}_{\text{data}}$, respectively. The general knowledge G is incorporated by defining an appropriate set of functions $g_\alpha(H_{\text{map}}, R_{\text{data}})$, as follows:

The knowledge of the mean $m_H(s)$ and $m_R(s)$ of $H(s)$ and $R(s)$, respectively, is obtained by selecting

$$g_i(H_{\text{i}}; s_i) = H_{\text{i}}; \qquad \bar{g}_i(s_i) = m_H(s_i), \quad i \in J_H \qquad (8.42)$$

$$g_i(R_{\text{i}}; s_i) = R_{\text{i}}; \qquad \bar{g}_i(s_i) = m_R(s_i), \quad i \in J_R, \qquad (8.43)$$

where $J_H = \{1,...,n_H\}$ and $J_R = \{n_H + 1,...,n\}$. The knowledge of the non-centered covariance functions $m_{RR}(s,s')$ and $m_{RR}(s,s')$ of $H(s)$ and $R(s)$, respectively, is obtained by selecting

$$g_{ij}(H_{\,\mathrm{i}}, H_{\,\mathrm{j}}; s_i, s_j) = H_{\,\mathrm{i}} H_{\,\mathrm{j}}; \qquad \bar{g}_{ij}(s_i, s_j) = m_{HH}(s_i, s_j), \quad i \in J_H, \ j \in J_H \tag{8.44}$$

$$g_{ij}(R_{\,\mathrm{i}}, R_{\,\mathrm{j}}; s_i, s_j) = R_{\,\mathrm{i}} R_{\,\mathrm{j}}; \qquad \bar{g}_{ij}(s_i, s_j) = m_{RR}(s_i, s_j), \quad i \in J_R, \ j \in J_R \tag{8.45}$$

The knowledge of the non-centered cross-covariance function $m_{HR}(s,s')$ between $H(s)$ and $R(s)$ is obtained by selecting

$$g_{ij}(H_{\,\mathrm{i}}, R_{\,\mathrm{j}}; s_i, s_j) = H_{\,\mathrm{i}} R_{\,\mathrm{j}}; \qquad \bar{g}_{ij}(s_i, s_j) = m_{HR}(s_i, s_j), \quad i \in J_H, \ j \in J_R \tag{8.46}$$

Additionally the fourth order moment $m_{R,4}(s)$ of $R(s)$ is included by selecting

$$g_{n+i}(R_{\,\mathrm{i}}; s_i) = R_{\,i}^{\,4}; \qquad \bar{g}_{n+i}(s_i) = m_{R,4}(s_i), \quad i \in J_R. \tag{8.47}$$

The constraints (8.42) to (8.47) are summarized in Table 8.1. The prior pdf incorporating the general knowledge of Table 8.1 is given by

$$f_G(H_{\,\mathrm{data}}, R_{\,\mathrm{map}}; s_1 \ldots s_n) = Z^{-1} \exp[\sum_{i \in J_H} \mu_i H_{\,\mathrm{i}} + \sum_{i \in J_R} \mu_i R_{\,\mathrm{i}} + \sum_{i \in J_H} \sum_{j \in J_H} \mu_{ij} H_{\,\mathrm{i}} H_{\,\mathrm{j}} + \sum_{i \in J_R} \sum_{j \in J_R} \mu_{ij} R_{\,\mathrm{i}} R_{\,\mathrm{j}} + \sum_{i \in J_H} \sum_{j \in J_R} \mu_{ij} H_{\,\mathrm{i}} R_{\,\mathrm{i}} + \sum_{i \in J_R} \mu_{i+n} R_{\,i}^{\,4}] \tag{8.48}$$

where the Lagrange coefficients μ_i's and μ_{ij}'s are obtained by solving the system of equations obtained from Table (1), i.e.

$$\begin{cases} \int dH_{\text{map}} \int dR_{\text{data}}\, H_{\text{i}}\, f_G(H_{\text{map}}, R_{\text{data}}; s_1 \ldots s_n) = m_H(s_i), \quad i \in J_H \\ \int dH_{\text{map}} \int dR_{\text{data}}\, R_{\text{i}}\, f_G(H_{\text{map}}, R_{\text{data}}; s_1 \ldots s_n) = m_R(s_i), \quad i \in J_R \\ \int dH_{\text{map}} \int dR_{\text{data}}\, H_{\text{i}} H_{\text{j}}\, f_G(H_{\text{map}}, R_{\text{data}}; s_1 \ldots s_n) = m_{HH}(s_i, s_j), \quad i \in J_H, j \in J_H \\ \int dH_{\text{map}} \int dR_{\text{data}}\, R_{\text{i}} R_{\text{j}}\, f_G(H_{\text{map}}, R_{\text{data}}; s_1 \ldots s_n) = m_{RR}(s_i, s_j), \quad i \in J_R, j \in J_R \\ \int dH_{\text{map}} \int dR_{\text{data}}\, H_{\text{i}} R_{\text{j}}\, f_G(H_{\text{map}}, R_{\text{data}}; s_1 \ldots s_n) = m_{HR}(s_i, s_j), \quad i \in J_H, j \in J_R \\ \int dH_{\text{map}} \int dR_{\text{data}}\, R_i^4\, f_G(H_{\text{map}}, R_{\text{data}}; s_1 \ldots s_n) = m_{R,4}(s_i), \quad i \in J_R \end{cases} \tag{8.49}$$

This system of equations has a solution for a given initial condition $q(s)$ and H_o, which is obtained using either analytical or numerical methods. The prior pdf (Eq. 8.49) incorporates the knowledge of the Darcy law, and it will serve as the basis to calculate the BME posterior pdf using hard and soft data.

TABLE 8.1: General knowledge constraints

α	g_α	$\bar{g}_\alpha$
$\alpha = i,\ i \in J_H$	$g_i(H_{\text{i}}; s_i) = H_{\text{i}}$	$\bar{g}_i(s_i) = m_H(s_i)$
$\alpha = i,\ i \in J_R$	$g_i(R_{\text{i}}; s_i) = R_{\text{i}}$	$\bar{g}_i(s_i) = m_R(s_i)$
$\alpha = (ij),\ i \in J_H,\ j \in J_H$	$g_{ij}(H_{\text{i}}, H_{\text{j}}; s_i, s_j) = H_{\text{i}} H_{\text{j}}$	$\bar{g}_{ij}(s_i, s_j) = m_{HH}(s_i, s_j)$
$\alpha = (ij),\ i \in J_R,\ j \in J_R$	$g_{ij}(R_{\text{i}}, R_{\text{j}}; s_i, s_j) = R_{\text{i}} R_{\text{j}};$	$\bar{g}_{ij}(s_i, s_j) = m_{RR}(s_i, s_j)$
$\alpha = (ij),\ i \in J_H,\ j \in J_R$	$g_{ij}(H_{\text{i}}, R_{\text{j}}; s_i, s_j) = H_{\text{i}} R_{\text{j}};$	$\bar{g}_{ij}(s_i, s_j) = m_{HR}(s_i, s_j)$
$\alpha = n + i\ ,\ i \in J_R$	$g_{n+i}(R_{\text{i}}; s_i) = R_i^4;$	$\bar{g}_{n+i}(s_i) = m_{R,4}(s_i)$

8.4.4. The BME Posterior PDF

Let $\boldsymbol{H}_{\text{hard}}^{\text{T}} = [H_1, \ldots, H_{m_{Hh}}]$, $\boldsymbol{H}_{\text{soft}}^{\text{T}} = [H_{m_{Hh}+1}, \ldots, H_{m_H}]$, and H_k represent $H(s)$ at the hard data points, soft data points and estimation points, respectively, such that

$\boldsymbol{H}_{\text{map}}^{\text{T}} = [\boldsymbol{H}_{\text{hard}}^{\text{T}}\, \boldsymbol{H}_{\text{soft}}^{\text{T}}\, H_k]$. Similarly let $\boldsymbol{R}_{\text{hard}}^{\text{T}} = [R_1,...,R_{m_{Rh}}]$ and $\boldsymbol{R}_{\text{soft}}^{\text{T}} = [R_{m_{Rh}+1},...,R_{m_R}]$ represent $R(s)$ at the hard and soft data points, respectively, such that $\boldsymbol{R}_{\text{data}}^{\text{T}} = [\boldsymbol{R}_{\text{hard}}^{\text{T}}\, \boldsymbol{R}_{\text{soft}}^{\text{T}}]$.

For soft data of the interval type, the BME posterior pdf is given by

$$f_K(H_k) = A^{-1} \int_{\boldsymbol{l}_H}^{\boldsymbol{u}_H} dH_{\text{soft}} \int_{\boldsymbol{l}_R}^{\boldsymbol{u}_R} dR_{\text{soft}}\, f_G(H_{\text{map}}, R_{\text{data}}), \tag{8.50}$$

where $\boldsymbol{l}_H$ and $\boldsymbol{u}_H$ are the lower and upper bounds of the soft data for hydraulic head such that $\boldsymbol{l}_H \le H_{\text{soft}} \le \boldsymbol{u}_H$, and $\boldsymbol{l}_R$ and $\boldsymbol{u}_R$ are the lower and upper bounds of the soft data for hydraulic resistivity such that $\boldsymbol{l}_R \le R_{\text{soft}} \le \boldsymbol{u}_R$.

In the case of the soft data of the probabilistic type, the BME posterior pdf is given by

$$f_K(H_k) = A^{-1} \int dH_{\text{soft}} \int dR_{\text{soft}}\, f_S(H_{\text{soft}}, R_{\text{soft}})\, f_G(H_{\text{map}}, R_{\text{data}}), \tag{8.51}$$

where $f_S(H_{\text{soft}}, R_{\text{soft}})$ represents the soft knowledge of probabilistic type.

8.4.5. Simulated Case Study

The covariance of hydraulic resistivity $R(s)$ is often modelled using an exponential function, given by

$$c_R(s,s') = c_R(r = |s'-s|) = c_{R,0} \exp(-r / a_R). \tag{8.52}$$

Using this model with $c_{R,0} = 1$ (sec/ mm)^2 and $a_R = 6$ m we generate the hydraulic resistivity profile $R(s)$ shown in Fig. 8.5b, where the distance between the grid points is

$0.5\ m$, and the mean of $R(s)$ is given by $m_R(s) = m_R = 2$ sec/ mm. The corresponding profile of hydraulic conductivity $K(s)$, given by $K(s) = 1/R(s)$, is shown in Fig. 8.5a. The distribution of values for $K(s)$ and $R(s)$ at those grid points is shown by means of the histograms of Fig. 8.6. The histogram of $K(s)$ values in Fig. 8.6a is asymmetric, with a tail of high values truncated at 5 mm/sec in the figure. The histogram of $R(s)$ values in Fig. 8.6b may be approximated by a symmetric pdf with a kurtosis coefficient $m_{R,4} / c_{R,0}^2$=3. Note that this simulated case study represent well certain types of soils (e.g. with skewed distribution of $K(s)$), but other situation may just as easily be explored by choosing the proper simulation parameters.

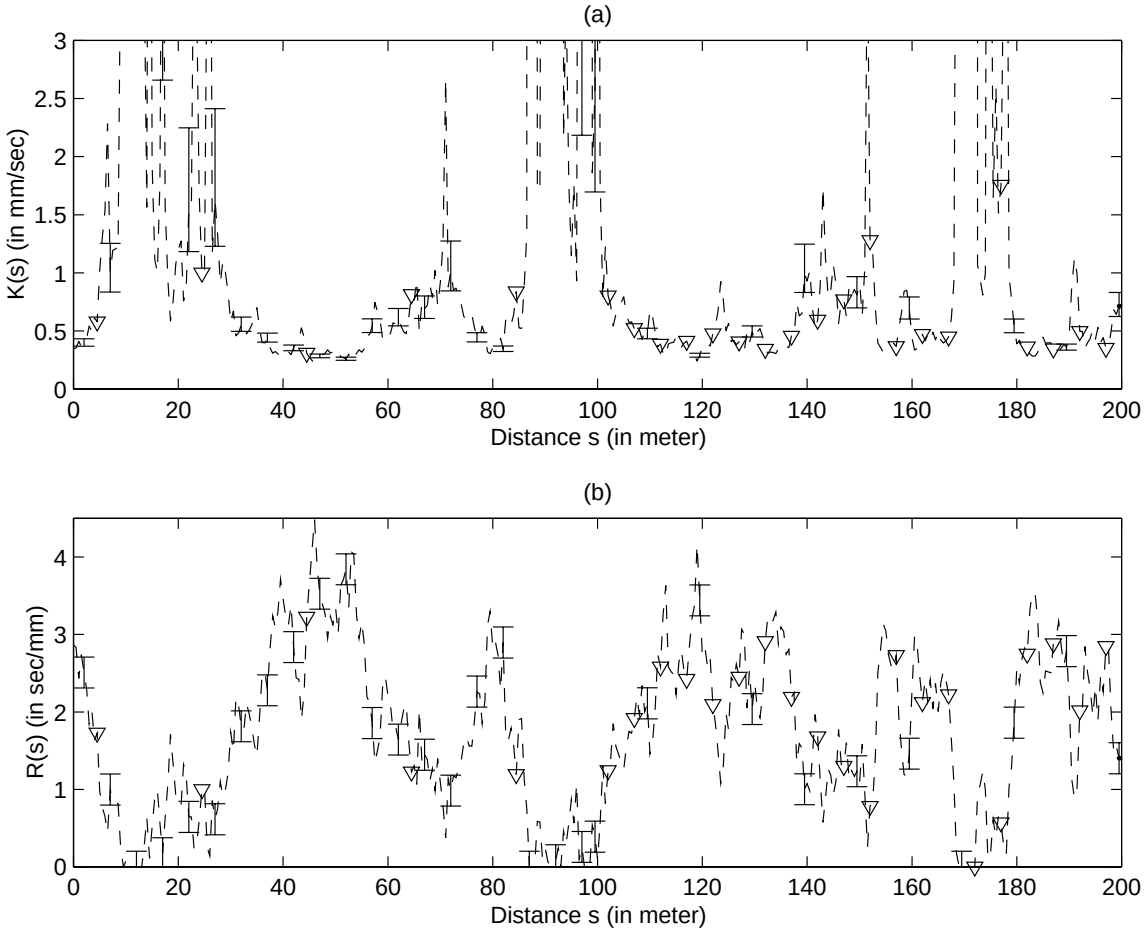

Figure 8.5: Simulated profile for (a) the hydraulic conductivity H(s), and (b) the hydraulic resistivity R(s). The hard data and soft interval data for test case 1 are shown with triangles and error bars, respectively.

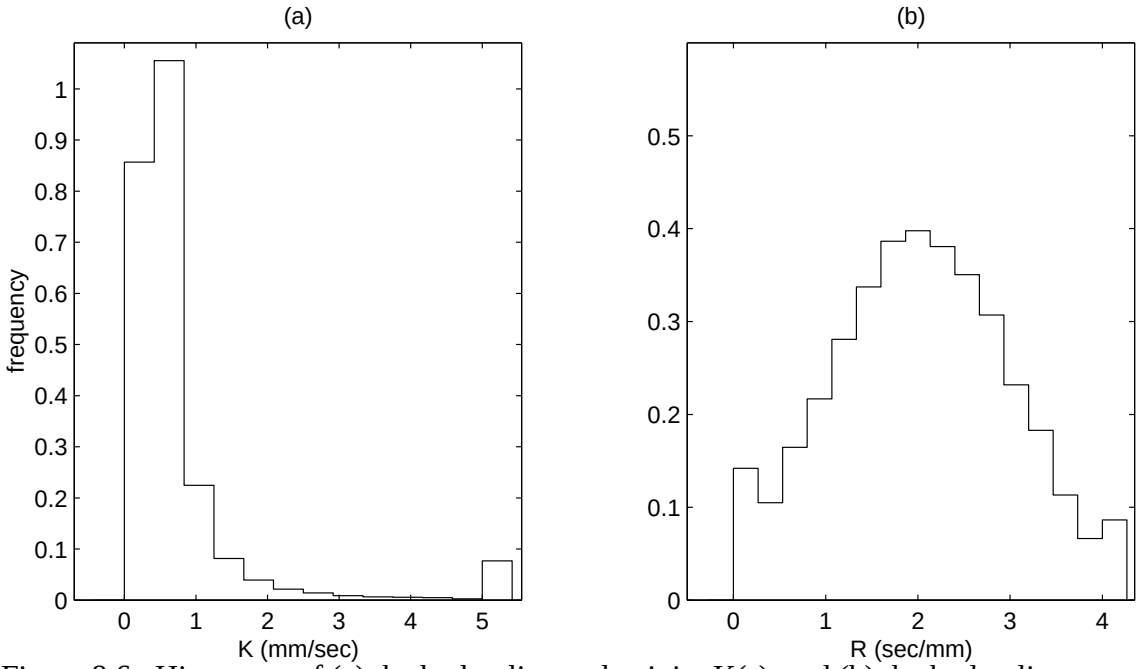

Figure 8.6: Histogram of (a) the hydraulic conductivity K(s), and (b) the hydraulic resistivity R(s).

The profile of hydraulic head calculated by solving the Darcy equation (8.31) using as boundary condition $H_0 = 100\ m$ and a constant specific discharge of $q(s) = q = 0.05\ mm/\sec$ is shown in Fig. 8.7a. The values of $H(s)$ at the grid-points were calculated by a numerical integration of the $K(s)$ data, and they are considered the "true" profile of hydraulic head. The mean hydraulic head $m_H(s) = H_o - q\, m_R\, s$ is shown with a dashed line in Fig. 8.7a, and the difference $H(s) - m_H(s)$ is called the hydraulic head fluctuation. The histogram of hydraulic head fluctuation is shown with plain lines in Fig. 8.7b for locations corresponding to $s = 5\ m$, $s = 25\ m$ and $s = 75\ m$. These histograms were obtained by using 2000 realizations of $H(s)$, and they show that the spread of the distribution of the hydraulic head fluctuations around 0 increases as the abscissa s gets further from the origin s=0, as expected due to the deterministic boundary condition at the origin.

(a) (b)

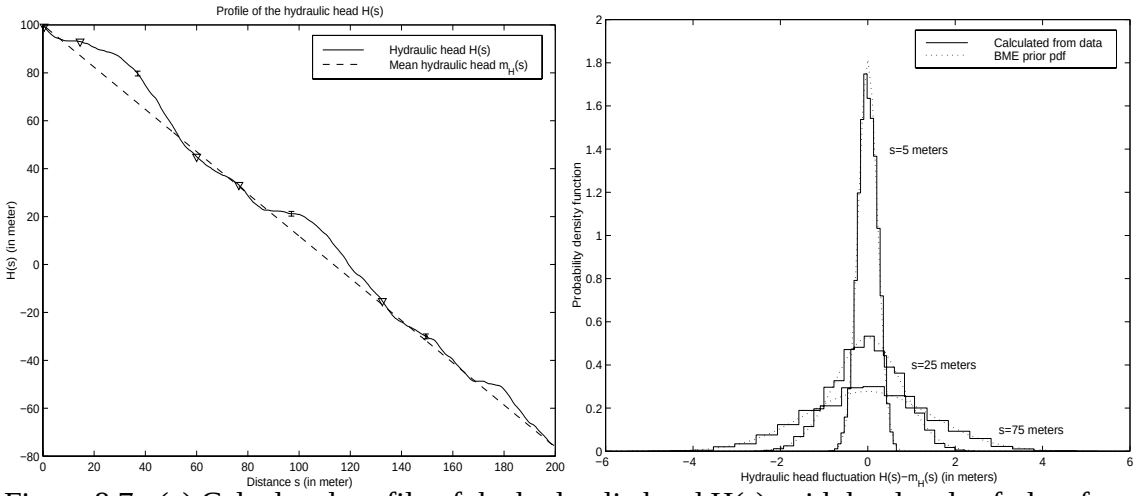

Figure 8.7: (a) Calculated profile of the hydraulic head H(s), with hard and soft data for test case 1 represented using triangles and error bars, respectively, (b) histogram of the hydraulic head at different location s.

In a first test case, we consider the estimation of the hydraulic head using sparse measurements of $H(s)$ and $R(s)$. The hard and soft (interval) data selected are shown with triangles and error bars, respectively, in Fig 8.5b for $R(s)$, and in Fig 8.7a for $H(s)$. Using only the hard and soft data we (re)estimate the hydraulic head along the flow domain, and we may then compare the estimated values with the simulated (true) profile. When estimating $H(s)$ we use different estimation methods for comparison purposes. The first method presented here is the classical Simple Kriging (SK) method, where only the hard data for $H(s)$ is used, and the covariance for $H(s)$ is given by an isotropic Gaussian model obtained by fitting the hydraulic head data. The estimated profile using SK is shown with a plain line in Fig. 8.8a, where the true profile is shown in dotted line. Note that this approach does not use the knowledge of the Darcy law and flow boundary condition, and furthermore it relies on the assumption that the hydraulic head fluctuations are homogeneous in space (i.e. have a constant mean and variance). This assumption is clearly not supported by the pdf of $H(s)$, shown in Fig 8.7b, which shows a marked increase of the variance of $H(s)$ as s increases.

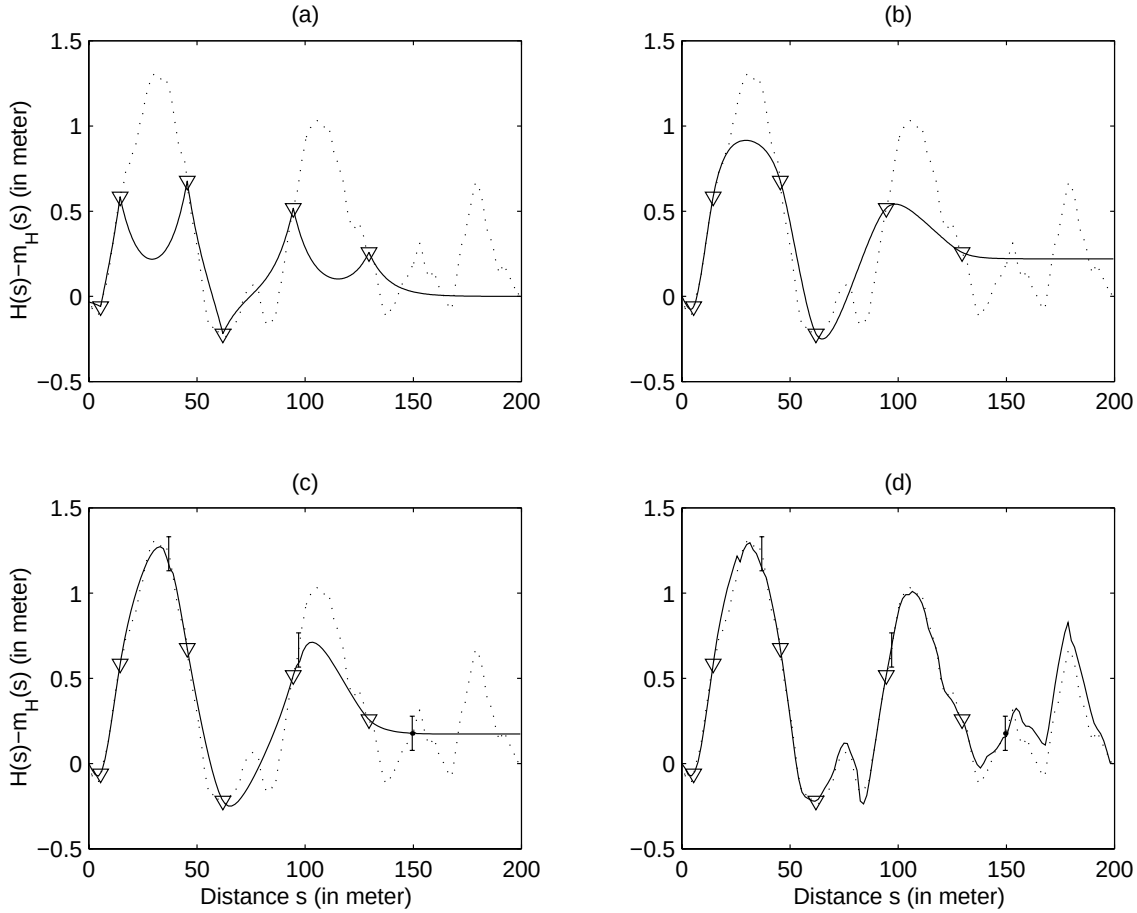

Figure 8.8: Estimated hydraulic head fluctuation $H(s) - m_H(s)$, obtained for test case 1 from (a) SK using hard data for H(s), (b) BME using hard data for H(s), (c) BME using hard and soft data for H(s), (d) BME using hard and soft data for both H(s) and R(s).

A better approach to estimate $H(s)$ is the BME method. In the BME method the general knowledge consists of the Darcy law, Eq. (8.31), the boundary conditions H_0 and q, and the moments of the hydraulic resistivity, m_R, $c_R(s,s')$, and $m_{R,4}$. Using this information, we calculate in the first stage of the BME method the prior pdf for the hydraulic head and hydraulic resistivity data. This stage is performed by numerically solving for the Lagrange coefficients (the μ_i's and μ_{ij}'s) of Eq. (8.49). Note that Eq. (8.49) is a set of non-linear equations that do not present any conceptual difficulty, however the multiple integrals have a high numerical complexity. In the case study presented here we assumed that kurtosis coefficient is given by $m_{R,4} / c_{R,0}^2$=3, so that μ_{i+n}=0, $i \in J_R$, and exact analytical expressions for the integrals may be derived. In the

more general case where $m_{R,4} / c_{R,0}^2 < 3$, it is possible to approximate the integrals with analytical expressions (Christakos, Hristopulos and Serre; 1999). For illustration purposes we plot in dotted line in Fig. 8.7b the prior pdf for the hydraulic head at points $s = 5\ m$, $s = 25\ m$ and $s = 75\ m$, and we note that they are in excellent agreement with the experimental histogram calculated from the data. The posterior pdf given by Eq. (8.51) is calculated using the prior pdf and the hard and soft data available. The BME mode estimate (i.e. the mode of the posterior pdf) is used to plot the estimated profile of hydraulic head fluctuation shown with a plain line in Fig. 8.8b to 8.8c. In Fig. 8.8b we show the estimate profile obtained using only hard data for $H(s)$ (i.e. the triangles of Fig. 8.8b). Note that the BME estimated profile of Fig. 8.8b is different than the SK estimated profile of Fig. 8.8a, because BME includes the knowledge of the Darcy law, while SK does not. In fact the BME estimate provides a better estimation of $H(s)$ than SK in the neighborhood the hard data points, and a more meaningful extrapolation at estimation points away from any hard data. Moreover the BME method allows to rigorously account for soft data of the interval type, as shown with error bars in Fig 8.8c. Using both hard and soft data for $H(s)$, the BME method provides an improved estimated profile, as shown in Fig. 8.8c. Finally by including the knowledge of the Darcy law, the BME method allows to also account for hard and soft data about $R(s)$. Using hard and soft data for $R(s)$ shown with triangles and error bars in Fig 8.5b, as well as the hard and soft data for $H(s)$, we obtain the estimated profile for the hydraulic head fluctuations shown in Fig. 8.8d. It is apparent from the figure that BME provides a substantial improvement over classical kriging methods.

In a second case study we consider the problem of estimation of the hydraulic resistivity $R(s)$ (or equivalently the hydraulic conductivity $K(s) = 1 / R(s)$) using sparse measurements of $R(s)$ and $H(s)$. This problem is sometime called the inverse problem, since we seek to obtain $R(s)$, considered the input, such that they are consistent with the

measured $H(s)$, considered the output with respect to solving the Darcy law. While it is possible to obtain accurate measurements of the hydraulic head $H(s)$, it is difficult to directly measure the hydraulic conductivity. Therefore, in the second case study, we consider that the measurements for $H(s)$ are the hard data shown with triangles in Fig. 8.9a, while the information for $R(s)$ consist of the soft interval data shown with error bars in Fig. 8.9b. For illustration purpose we calculate the BME estimate for three different mapping situations. In the first mapping situation we assume that the specificatory knowledge consists of only the soft data for $R(s)$, and we show the corresponding BME estimated profile for $R(s)$ in Fig. 8.9b. Note that this type of soft information arises commonly when estimating the hydraulic conductivity, and the BME method provides a rigorous framework to account for soft information. In the second mapping situation we consider that the specificatory knowledge includes both the soft data for $R(s)$, as well as the hard data for $H(s)$ shown with triangles in Fig. 8.9a. Using this information we obtain the estimated profile shown in Fig. 8.9c. It is apparent from the figure that this estimated profile provides a substantial improvement over that of Fig. 8.9b. Note that the estimated profile of Fig. 8.9c respects the soft information, but also reproduces the important features of the true resistivity profile shown in dotted line. This unique feature of the BME approach is due to the fact that BME accounts for the knowledge of the Darcy law which relates $H(s)$ and $R(s)$, leading to substantial improvement of the estimated hydraulic resistivity. Finally in Fig. 8.9d we show the estimated profile for $R(s)$ using only the hard data for $H(s)$ (the triangles of Fig. 8.9a). We note that in this case the important features of the hydraulic resistivity profiles are well represented.

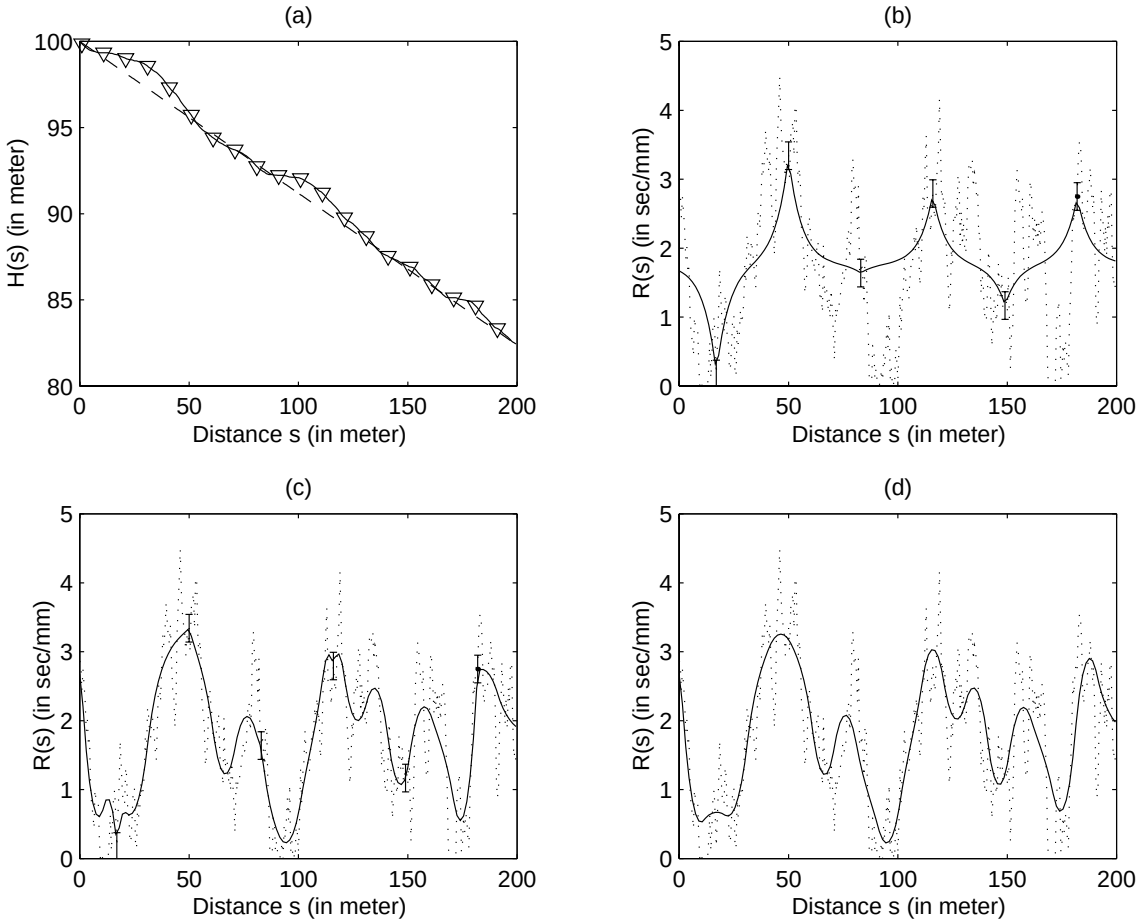

Figure 8.9: (a) Calculated profile of the hydraulic head H(s), with hard data for test case 2 represented using triangles, and estimated hydraulic resistivity R(s) for test case 2, obtained from (b) BME using data for R(s), (c) BME using data for both R(s) and H(s), (d) BME using only data for H(s).